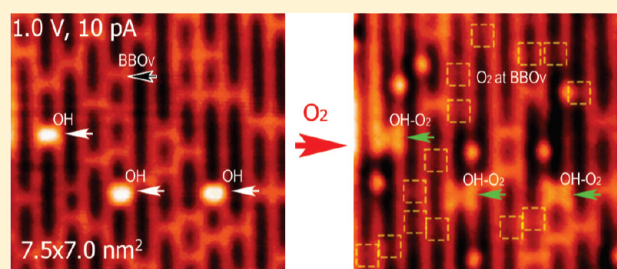


# Molecular Oxygen Adsorption Behaviors on the Rutile $\text{TiO}_2(110)$ - $1 \times 1$ Surface: An in Situ Study with Low-Temperature Scanning Tunneling Microscopy

Shijing Tan, Yongfei Ji, Yan Zhao, Aidi Zhao, Bing Wang,\* Jinlong Yang, and J.G. Hou\*

Hefei National Laboratory for Physical Sciences at the Microscale, University of Science and Technology of China, Hefei 230026, Anhui, China

**ABSTRACT:** A knowledge of adsorption behaviors of oxygen on the model system of the reduced rutile  $\text{TiO}_2(110)$ - $1 \times 1$  surface is of great importance for an atomistic understanding of many chemical processes. We present a scanning tunneling microscopy (STM) study on the adsorption of molecular oxygen either at the bridge-bonded oxygen vacancies ( $\text{BBO}_V$ ) or at the hydroxyls (OH) on the  $\text{TiO}_2(110)$ - $1 \times 1$  surface. Using an in situ  $\text{O}_2$  dosing method, we are able to directly verify the exact adsorption sites and the dynamic behaviors of molecular  $\text{O}_2$ . Our experiments provide direct evidence that an  $\text{O}_2$  molecule can intrinsically adsorb at both the  $\text{BBO}_V$  and the OH sites. It has been identified that, at a low coverage of  $\text{O}_2$ , the singly adsorbed molecular  $\text{O}_2$  at  $\text{BBO}_V$  can be dissociated through an intermediate state as driven by the STM tip. However, singly adsorbed molecular  $\text{O}_2$  at OH can survive from such a tip-induced effect, which implies that the singly adsorbed  $\text{O}_2$  at OH is more stable than that at  $\text{BBO}_V$ . It is interesting to observe that when the  $\text{BBO}_V$ s are fully filled with excess  $\text{O}_2$  dosing, the adsorbed  $\text{O}_2$  molecules at  $\text{BBO}_V$  tend to be nondissociative even under a higher bias voltage of 2.2 V. Such a nondissociative behavior is most likely attributed to the presence of two or more  $\text{O}_2$  molecules simultaneously adsorbed at a  $\text{BBO}_V$  with a more stable configuration than singly adsorbed molecular  $\text{O}_2$  at a  $\text{BBO}_V$ .



## 1. INTRODUCTION

The adsorption of molecular oxygen on titanium dioxide has attracted extensive study interests since adsorbed oxygen plays an important role in many surface chemical processes,<sup>1–3</sup> particularly for the low-temperature oxidation reactions in heterogeneous catalysis,<sup>4</sup> as well as in photocatalysis.<sup>5</sup> In general, adsorbed  $\text{O}_2$  acts as a scavenger to excess electrons originating from donor-specific sites, such as bridge-bonded oxygen vacancies ( $\text{BBO}_V$ ), hydroxyl groups (OH), and Ti interstitials.<sup>6–15</sup> Scanning tunneling microscopy (STM) has been used to characterize adsorbed molecules on the  $\text{TiO}_2$  surface and provide useful information for understanding the chemical processes at the atomic scale. Some recent efforts using STM have been made to understand the adsorption of molecular oxygen on the reduced rutile  $\text{TiO}_2(110)$ - $1 \times 1$  surface.<sup>12,16</sup> However, adsorption of molecular oxygen at low temperatures remains a puzzling problem.<sup>7,8,14,17–20</sup> The STM results showed dissociative  $\text{O}_2$ , either dissociated at  $\text{BBO}_V$  with one O atom healing the  $\text{BBO}_V$  and the other O atom leaving at a neighboring 5-fold-coordinated Ti ( $\text{Ti}_{5c}$ ) site as an adatom,<sup>18,20–22</sup> or dissociated directly at  $\text{Ti}_{5c}$  sites, yielding paired O adatoms which may be caused by Ti interstitials.<sup>7,23</sup> It was reported that the  $\text{O}_2$  molecule may also react with the hydroxyl group, yielding  $\text{HO}_2$  species.<sup>9,24–26</sup> On the other hand, the photodesorption experiments indicate two states of molecular  $\text{O}_2$  at  $\text{BBO}_V$ .<sup>6</sup> The temperature-programmed desorption (TPD) measurements suggest that up to three  $\text{O}_2$

molecules adsorb per  $\text{BBO}_V$  at 120 K, but a dissociation channel is favored above 150 K.<sup>8</sup> A recent result reports that two  $\text{O}_2$  molecules chemisorb per  $\text{BBO}_V$  and convert to a stable tetra-oxygen as annealed above 200 K,<sup>27</sup> which was predicted by the theoretical results.<sup>28</sup> In photocatalysis, it is reported that the molecular oxygen plays an indispensable role, assisting the charge separation and generating the active species of  $\text{O}_2^-$ ,  $\text{O}_2^{2-}$ ,  $\text{HO}_2$ , etc.<sup>9,29–31</sup> Such molecular oxygen species on  $\text{TiO}_2$  are required to be comprehensively understood at a molecular scale, especially on their actual adsorption sites, in the interaction with the  $\text{TiO}_2$  surface, and in the reaction with other adsorbed species.

In this study, we investigated  $\text{O}_2$  adsorption on  $\text{TiO}_2(110)$  surfaces with  $\text{BBO}_V$  and OH. The adsorption behaviors of molecular  $\text{O}_2$  were systematically studied with various coverages of  $\text{O}_2$  and different temperatures using STM. The dissociation of  $\text{O}_2$  molecules at  $\text{BBO}_V$  was measured at different temperatures and different  $\text{O}_2$  coverages. The dissociation processes are analyzed and simulated using first-principle calculations. The interaction of  $\text{O}_2$  with OH is also studied, which shows a behavior different from that of adsorbed  $\text{O}_2$  at  $\text{BBO}_V$ . Our study provides a comprehensive picture of  $\text{O}_2$  adsorption and some insights into the role of  $\text{O}_2$  as a scavenger to excess electrons in the chemical reactions mediated by  $\text{TiO}_2$  surfaces.

Received: November 18, 2010

Published: January 19, 2011

## 2. EXPERIMENTAL SECTION

The experiments were conducted in an ultra-high-vacuum low-temperature STM (LT-STM) system (Omicron, base pressure  $<3 \times 10^{-11}$  mbar). The reduced rutile  $\text{TiO}_2(110)-1\times1$  surface was prepared by repeated cycles of 1000 eV of  $\text{Ar}^+$  sputtering and annealing to 900 K with a Ta-foil heater behind the sample. The clean  $\text{TiO}_2(110)-1\times1$  surface was then transferred to the cryostat of the microscope, which had been precooled to 80 or 5.2 K. The STM measurements were performed mostly at 80 and 5.2 K, at which the microscope has good performance in thermal stability. Variable-temperature experiments have also been performed by warming the sample from 80 to 130 K. The  $\text{O}_2$  (99.999%) dosing was performed by keeping the sample either at 80 K or at 5.2 K. During  $\text{O}_2$  dosing, the tip was retracted from the surface by about 10  $\mu\text{m}$ .

## 3. COMPUTATIONAL DETAILS

All the calculations were performed with the Vienna ab initio simulation package (VASP) with the generalized gradient approximation of Perdew, Burke, and Ernzerhof (PBE-GGA).<sup>32–35</sup> The  $\text{TiO}_2(110)-1\times1$  surface was modeled by periodically repeated slabs consisting of a  $4\times2$  cell with five O–Ti–O trilayers separated by 15 Å of vacuum. One of the bridge-bonded oxygen atoms in the uppermost layer was removed to mimic the oxygen vacancy. A plane-wave basis set with an energy cutoff of 460 eV and the projector-augmented wave (PAW) potential were employed.<sup>36</sup> Monkhorst-3 Pack grids of  $2\times2\times1$   $K$ -points were used. During the optimization, only atoms in the upper two trilayers were allowed to relax until the self-consistent forces were smaller than 0.01 eV/Å. The STM images were simulated by the Tersoff–Hamann formula.<sup>37,38</sup>

## 4. RESULTS AND DISCUSSION

**4.1. Adsorption of Molecular  $\text{O}_2$  at  $\text{BBO}_V$  with a Low Coverage.** Parts a and b of Figure 1 give a pair of images for the reduced  $\text{TiO}_2(110)-1\times1$  surface before and after the exposure of 0.04 langmuir of  $\text{O}_2$  (1 langmuir =  $1.33 \times 10^{-6}$  mbar·s). Figure 1a shows a typical empty-state STM image of reduced  $\text{TiO}_2(110)-1\times1$ , with alternating rows of 5-fold-coordinated Ti atoms ( $\text{Ti}_{5c}$ ) as bright rows and 2-fold-coordinated bridge-bonded O atoms ( $\text{BBO}$ ) as dark rows. The bright protrusions in the BBO rows are the oxygen vacancies ( $\text{BBO}_V$ ) with a concentration of 0.08 monolayer (1 monolayer =  $5.2 \times 10^{14}$  cm $^{-2}$ ). It is observed that after  $\text{O}_2$  dosing some of the  $\text{BBO}_V$ s become almost misty (marked by squares), and four  $\text{BBO}_V$ s remain in the frame, as shown in Figure 1b. The two bright protrusions at  $\text{Ti}_{5c}$  sites (marked by yellow arrows) are attributed to the O adatoms resulting from the dissociative  $\text{O}_2$  at  $\text{BBO}_V$ .<sup>14,20</sup> Parts c–f of Figure 1 correspondingly give the line profiles along marked lines 1–4 in Figure 1a and marked lines 1'–4' in Figure 1b. The apparent height of  $\text{BBO}_V$  changes from about 0.30 Å to a value of about 0.13 Å after  $\text{O}_2$  dosing. The observation here suggests that the misty  $\text{BBO}_V$  can be the adsorption of one molecule of  $\text{O}_2$ . To support this, we calculated the adsorbed configuration and simulated the image of the adsorbed molecular  $\text{O}_2$  at  $\text{BBO}_V$  with a  $4\times2$  unit cell including five O–Ti–O trilayers separated by 15 Å of vacuum based on the basis of density functional theory (DFT). Consistent with the previous calculated results,<sup>10,11,39,40</sup> the  $\text{O}_2$  molecule adsorbs at  $\text{BBO}_V$  with the bond axis perpendicular to the BBO row, as shown in Figure 1g. The O–O bond length is 1.44 Å, which is much longer than the bond length of  $\text{O}_2$  in the gas phase, suggesting that the molecular  $\text{O}_2$  at  $\text{BBO}_V$  is doubly charged as  $\text{O}_2^{2-}$ .<sup>10</sup> Figure 1h shows the simulated STM image, which exhibits a faint contrast for the

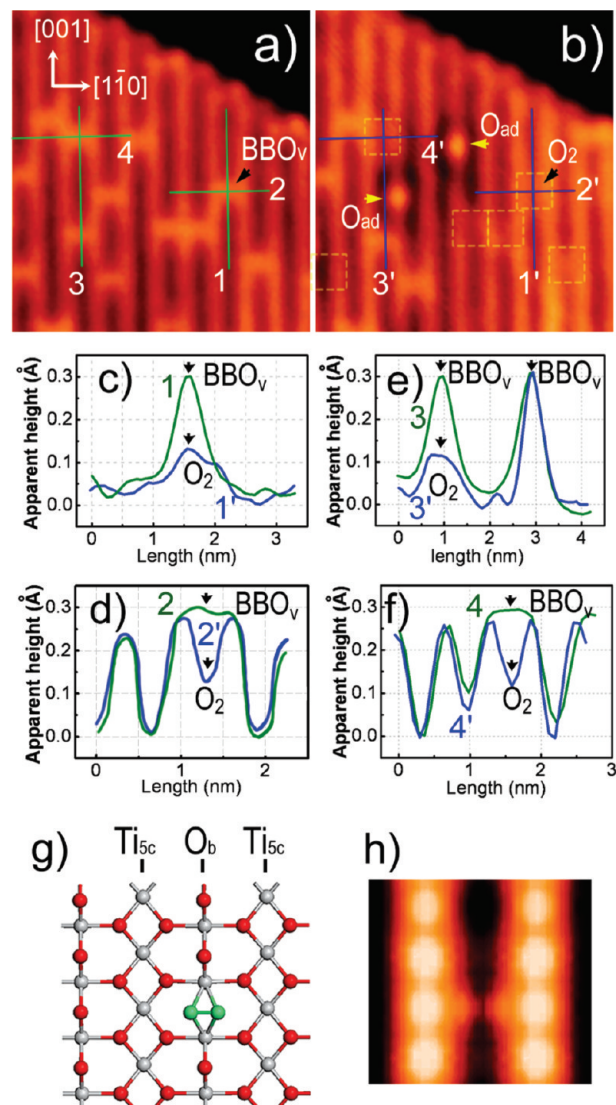


**Figure 1.** STM images of the hydroxyl-free  $\text{TiO}_2(110)-1\times1$  surface (a) before and (b) after 0.04 langmuir of  $\text{O}_2$  dosing within the same area ( $6.5 \times 7.0$  nm $^2$ , imaged at 1.0 V and 10 pA, at 80 K). The dashed squares mark the misty  $\text{BBO}_V$  after  $\text{O}_2$  dosing. The yellow arrows mark the O adatoms at  $\text{Ti}_{5c}$  sites. (c–f) Line profiles giving the relative apparent height change along lines 1–4 marked in (a) and lines 1'–4' marked in (b), correspondingly. (g) Optimized structure of molecular  $\text{O}_2$  adsorbed at  $\text{BBO}_V$  in top view. (h) Simulated STM image of molecular  $\text{O}_2$  adsorbed at  $\text{BBO}_V$  with a sample bias of 1.0 V (the Fermi level is set to be 0.12 eV below the conduction band minimum) and a constant height of 3.1 Å.

adsorbed  $\text{O}_2$  molecule at  $\text{BBO}_V$ , in good agreement with our experimental observations. Hence, Figure 1b provides the direct image of the singly adsorbed molecular  $\text{O}_2$  at  $\text{BBO}_V$  by comparison *in situ* with the image in Figure 1a.

**4.2. Adsorption of Molecular  $\text{O}_2$  with Variable Coverages.** Figure 2 shows the results obtained from the stepwise  $\text{O}_2$  exposure experiment. In the first step, we allowed the sample to be exposed to 0.02 langmuir of  $\text{O}_2$ . Figure 2b shows the first scanning frame after exposure of  $\text{O}_2$ . One can see three misty  $\text{BBO}_V$ s, similar to the image in Figure 1b. However, in addition to the misty  $\text{BBO}_V$ s, there are some paired protrusions occurring at the neighboring  $\text{Ti}_{5c}$  sites in opposite rows of the preexisting

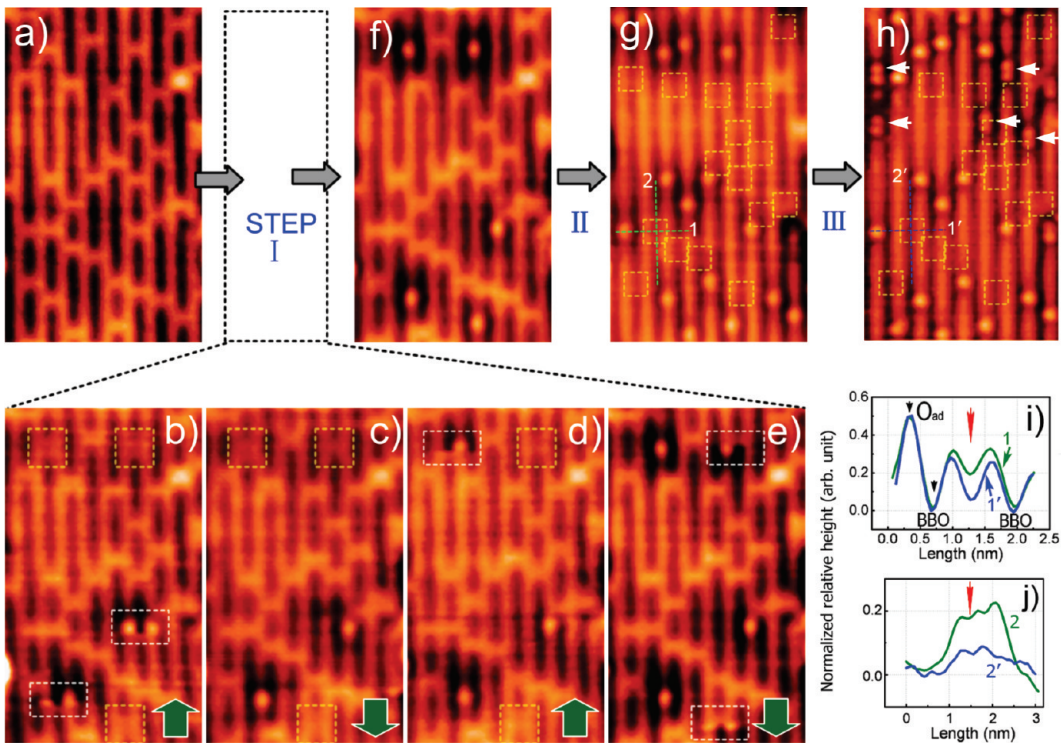


**Figure 2.** STM images obtained from a stepwise  $O_2$  adsorption process within the same area ( $5.7 \times 9.7 \text{ nm}^2$ , imaged at  $1.0 \text{ V}$  and  $10 \text{ pA}$ ,  $80 \text{ K}$ ). (a) Image before  $O_2$  dosing. (b–f) Consecutively acquired images after  $0.02$  langmuir of  $O_2$  dosing, showing the dissociation of the adsorbed  $O_2$  during scanning (step I). The green arrows show the scanning directions. (g) Image showing the fully filled  $\text{BBO}_V$  after an additional  $0.12$  langmuir of  $O_2$  dosing (step II). (h) Image acquired after another additional  $0.20$  langmuir of  $O_2$  dosing (step III). Dashed squares mark the misty  $\text{BBO}_V$  with adsorbed molecular  $O_2$ , dashed rectangles the intermediate state of the adsorbed molecular  $O_2$  at  $\text{BBO}_V$ , and white arrows the paired  $O$  adatoms presented at  $\text{Ti}_{5c}$  sites. (i, j) Line profiles corresponding to crossed lines 1 and 2 in (g) and lines 1' and 2' in (h). The red arrow denotes the crosspoint of the two lines.

$\text{BBO}_V$ s (marked by rectangles). As we show below, such protrusions can be attributed to an intermediate state of an adsorbed  $O_2$  molecule. Hence, there are five adsorbed  $O_2$  molecules in the image. After several cycles of consecutive scanning within the same area at a bias of  $1.0 \text{ V}$ , all five adsorbed  $O_2$  molecules dissociate and present five  $O$  adatoms at the neighboring  $\text{Ti}_{5c}$  sites (Figure 2b–f). In the second step, we allowed the sample to be further exposed to an additional  $0.12$  langmuir of  $O_2$ , as shown in Figure 2g. It is observed that all of the  $\text{BBO}_V$ s are filled by adsorbed  $O_2$ , accompanied by some more dissociative  $O_2$  that exhibits as  $O$  adatoms at  $\text{Ti}_{5c}$  sites. In the following step, the sample was exposed to another additional  $0.20$  langmuir of  $O_2$ . Some paired protrusions at the same  $\text{Ti}_{5c}$  row occur, as marked by the white arrows in Figure 2h. Such types of paired protrusions at the  $\text{Ti}_{5c}$  row have been observed before,<sup>14</sup> which have been attributed to dissociative  $O_2$  at  $\text{Ti}_{5c}$ .<sup>7</sup>

It is suggested that two  $O_2$  molecules chemisorb per  $\text{BBO}_V$  and convert to a stable tetraoxigen as annealed above  $200 \text{ K}$ , and the tetraoxigen can sustain upon annealing to  $400 \text{ K}$ .<sup>27,28</sup> As shown in Figure 2g,h, even though the  $\text{BBO}_V$ s are fully filled by adsorbed  $O_2$  with excess  $O_2$  dosing, it is difficult to obtain the exact number of adsorbed  $O_2$  molecules per  $\text{BBO}_V$  from the image. In Figure 2b–f, it is shown that the adsorbed  $O_2$  at a low coverage can be completely dissociated after repeated scanning at  $1.0 \text{ V}$  within the same area, which can be attributed to the fact that a singly adsorbed  $O_2$  at  $\text{BBO}_V$  is quite dissociative.<sup>31</sup> However, the image shown in Figure 2h did not follow the same behavior. With repeated scanning at  $1.0 \text{ V}$  and even at a high bias up to  $2.2 \text{ V}$ , we observed that the number of  $O$  adatoms and the main

feature of the surface almost remained unchanged, indicating that the adsorbed  $O_2$  molecules tend to be nondissociative, in contrast to the easily dissociated singly adsorbed  $O_2$  molecules at bias voltages higher than  $1.2 \text{ V}$  in our experiment. This phenomenon may lead to different explanations. First, one may think that it is due to the total desorption of the adsorbed molecules without dissociation. This argument can be ruled out, since in such a way the preexisting  $\text{BBO}_V$  should be recovered. Second, the adsorbed  $O_2$  may go through dissociation without leaving an  $O$  adatom at such a high coverage, but this is obviously inconsistent with the dissociation behavior of singly adsorbed  $O_2$ . A more plausible explanation is that the nondissociative  $O_2$  may contain quite stable oxygen adsorbates with a configuration quite different from that of the singly adsorbed  $O_2$  molecule.

To clarify, a further analysis is made by comparing the relative heights, for example, along the dashed green and blue lines in Figure 2g,h, respectively, as shown in Figure 2i,j. The line profiles have been normalized according to the height difference between the  $O$  adatom and the  $\text{BBO}$  row. It is observed that both profiles of lines 1 and 1' are almost overlapped, except for the range around the molecular  $O_2$  adsorption site, marked by the red arrow. In this range line 1' drops to a lower relative height, but not to the same height as the neighboring  $\text{BBO}$  rows (Figure 2i). Comparison of the line profiles along lines 2 and 2' shows that both lines also exhibit heights different from those of the other sites in the same  $\text{BBO}$  row, and line 2 is more protruded than line 2' around the range marked by the red arrow in Figure 2j. Considering its similarity (lines 1 and 2) to the singly adsorbed molecular  $O_2$  shown above, we suggest that it is a singly adsorbed  $O_2$  molecule

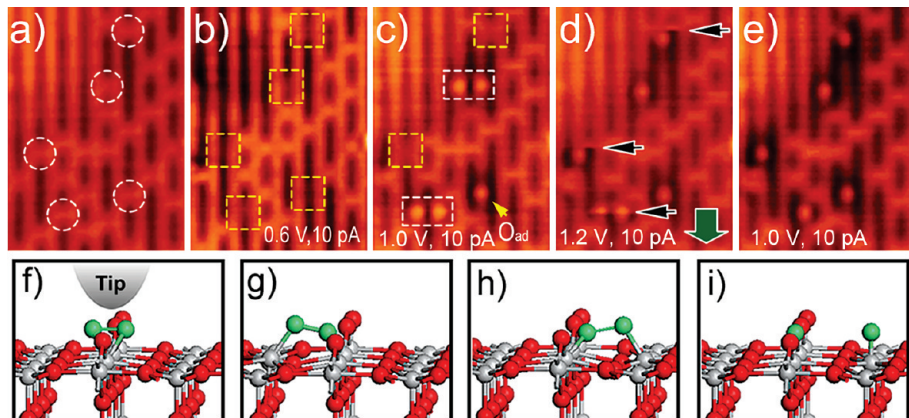


**Figure 3.** (a) Image of the bare  $\text{TiO}_2(110)$ - $1\times 1$  surface (size  $5.2 \times 7.2 \text{ nm}^2$ , acquired at  $1.0 \text{ V}$  and  $10 \text{ pA}$ ). Dashed circles mark the original  $\text{BBO}_V$  sites. (b–e) Images acquired after 0.02 langmuir of  $\text{O}_2$  dosing, acquired at different bias voltages. Squares mark  $\text{BBO}_V$  with adsorbed molecular  $\text{O}_2$  and rectangles the intermediate state of the adsorbed  $\text{O}_2$ . Dark arrows in (d) mark the scratches, and the green arrow denotes the scanning direction. Schematic drawings showing (f) molecular  $\text{O}_2$  under the tip at its equilibrium site, (g) molecular  $\text{O}_2$  inclined to the left  $\text{Ti}_{5c}$  site, (g) molecular  $\text{O}_2$  inclined to the right  $\text{Ti}_{5c}$  site, and (i) dissociative  $\text{O}_2$ .

at the corresponding  $\text{BBO}_V$  site in Figure 2g. Even though it becomes much dimmer in Figure 2h, the line profiles (line 1' and 2') show that it is different from a singly adsorbed molecule, but also different from a bare  $\text{BBO}_V$  site. Considering that the total  $\text{O}_2$  exposure is about 0.34 langmuir for Figure 2h, doubled compared to the  $\text{O}_2$  exposure of 0.14 langmuir for Figure 2g, we tend to believe that the  $\text{BBO}_V$  should adsorb simultaneously two or more  $\text{O}_2$  molecules, which may imply the existence of a stable configuration with more adsorbed molecules per  $\text{BBO}_V$ , as suggested before.<sup>27,28</sup>

**4.3. STM-Tip-Induced Dissociation of Adsorbed Molecular  $\text{O}_2$  at  $\text{BBO}_V$ .** The results in the previous STM studies showed dissociative  $\text{O}_2$ , dominantly with one  $\text{O}$  atom healing the  $\text{BBO}_V$  and the other  $\text{O}$  atom leaving at the neighboring  $\text{Ti}_{5c}$  site as an adatom.<sup>18,20–22</sup> Here, we observed that the dissociation of  $\text{O}_2$  is induced by the STM tip at a low  $\text{O}_2$  coverage, in which molecular  $\text{O}_2$  singly adsorbs at each  $\text{BBO}_V$  dominantly. We found that the singly adsorbed  $\text{O}_2$  at  $\text{BBO}_V$  may survive from the tip-induced dissociation when we applied relatively low bias voltages. In Figure 3, we give another set of experimental results. Figure 3b, acquired with a low bias voltage of  $0.6 \text{ V}$  after the exposure of 0.02 langmuir of  $\text{O}_2$ , shows a quite similar behavior of adsorbed  $\text{O}_2$  at  $\text{BBO}_V$ . We allowed a repeated scanning in the same area at the bias of  $0.6 \text{ V}$ . It is observed that the misty  $\text{BBO}_V$ s almost remain unchanged at this bias. However, when the bias is increased to about  $1.0 \text{ V}$ , it is observed that some of the adsorbed  $\text{O}_2$  molecules at  $\text{BBO}_V$  undergo dissociation and produce  $\text{O}$  adatoms at neighboring  $\text{Ti}_{5c}$  sites, as shown in Figure 3c. Interestingly, it is also observed that some paired protrusions occur at opposite  $\text{Ti}_{5c}$  sites neighboring the adsorbed  $\text{O}_2$  at the  $\text{BBO}_V$  (marked by the rectangles), similar to those in Figure 2b. Such paired protrusions should be an intermediate state of the molecular  $\text{O}_2$  before it dissociates. On the basis of our DFT calculations, such an intermediate state can be attributed to the inclined configuration, in good agreement with the theoretical prediction,<sup>39,40</sup> as shown by the schematic drawings in Figure 3f–h. Energetically, the flat-lying configuration in Figure 3f is more preferred than the inclined configuration in Figure 3g (or equivalently in Figure 3h) by about  $0.15 \text{ eV}$ . The barrier from the flat-lying configuration to the inclined configuration is about  $0.5 \text{ eV}$ , and the return barrier is small at  $0.35 \text{ eV}$ .<sup>39</sup> Thus, the

paired protrusions are suggested to be a switching behavior between the inclined configuration and the flat-lying equilibrium configuration, which is excited by the inelastic tunneling electron (IETE).<sup>41</sup> With the bias further increased to  $1.2 \text{ V}$ , the adsorbed  $\text{O}_2$  molecules at  $\text{BBO}_V$  have much higher probability to be dissociated. As shown in Figure 3d, one can see some scratches around the  $\text{BBO}_V$  with adsorbed  $\text{O}_2$  (marked by the dark arrows). The green arrow shows the scanning direction. In principle, the scratches reflect the very fast switching situation of the adsorbed  $\text{O}_2$  between the equilibrium state and the intermediate state. At  $80 \text{ K}$ , once a scratch was observed for the adsorbed  $\text{O}_2$  at  $\text{BBO}_V$ , consequently the  $\text{O}$  adatoms presented without observation of the intermediate state. This can be rationalized as follows: At a higher bias, the molecularly adsorbed  $\text{O}_2$  may have a higher probability to overcome the barrier to the metastable intermediate state with the inclined configuration, caused by the IETE with higher energies when the higher bias voltage is applied. With the inclined configuration,  $\text{O}_2$  can be dissociated easily by the IETE with higher energies also, resulting in the dissociation state (Figure 3e and the schematic drawing in Figure 3i). On the basis of the spin-polarized DFT calculations by Chrétien et al.,<sup>40</sup>  $\text{O}_2$  dissociation at  $\text{BBO}_V$  is exothermic by  $0.85 \text{ eV}$  in the triplet state and the highest barrier is  $0.67 \text{ eV}$ , and  $\text{O}_2$  dissociation is endothermic by  $0.11 \text{ eV}$  in the singlet state and the barrier is  $1.30 \text{ eV}$ . According to the dissociation dependence on the bias voltage in our experimental results (see Figure 5), the  $\text{O}_2$  dissociation is obviously observed at a voltage of about  $0.8 \text{ V}$  at  $80 \text{ K}$ , which suggests most likely that the adsorbed  $\text{O}_2$  is in the triplet state and the  $\text{O}_2$  dissociation is through the exothermic process.

To confirm the suggestion that the adsorbed  $\text{O}_2$  may switch between the different configurations, we measured the tunneling-current ( $I-t$ ) curve by locating the tip over the adsorbed  $\text{O}_2$  molecule. An  $I-t$  curve is recorded by locating the STM tip over a specific site and turning off the feedback loop of the STM without scanning. At  $80 \text{ K}$ , the  $I-t$  curve did not give obvious signals showing the switching state. This may be caused by a too fast switching rate to be recorded in the STM images and the  $I-t$  curves at  $80 \text{ K}$ . We then cooled the sample to  $5.2 \text{ K}$ . Figure 4 shows some representative  $I-t$  curves acquired at different bias voltages at  $5.2 \text{ K}$ . Figure 4a shows the  $I-t$  curve acquired at the bias of  $1.2 \text{ V}$  and the set point current of  $10 \text{ pA}$  at a misty  $\text{BBO}_V$

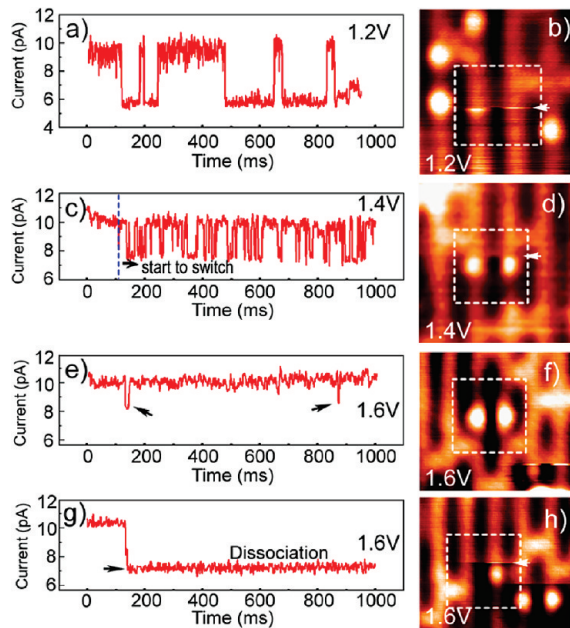


**Figure 4.** Representative  $I-t$  curves and STM images acquired at different bias voltages at 5.2 K: (a, b) at 1.2 V and 10 pA, (c, d) at 1.4 V and 10 pA, (e, f) at 1.6 V and 10 pA, (g, h) at 1.6 V and 10 pA. The  $I-t$  curves are acquired at the center of the adsorbed  $O_2$ . The images are selected from the large scanning areas correspondingly at the bias voltages and the set point currents indicated. Image sizes: (b)  $2.6 \times 2.8 \text{ nm}^2$ , (d)  $2.8 \times 3.0 \text{ nm}^2$ , (f)  $3.4 \times 3.1 \text{ nm}^2$ , (h)  $3.4 \times 3.0 \text{ nm}^2$ .

with an adsorbed molecule of  $O_2$ . The high current state in the  $I-t$  curve thus denotes the  $O_2$  molecule under the tip at its equilibrium adsorption site, while the low current state denotes the  $O_2$  molecule off the tip. Correspondingly, we found the behavior of the adsorbed  $O_2$  in the STM images, as shown in Figure 4b. It is noted that as marked by the arrow the bright notches at the two opposite  $Ti_{Sc}$  rows are not in the same scanning line, reflecting the  $O_2$  either at the left or at the right side of its equilibrium sites. In this case, the adsorbed  $O_2$  molecule mainly stays at its equilibrium site and has a small probability to be excited to either off state as shown in Figure 3g,h. At 1.4 V, the switching rate increases significantly, roughly higher than that at 1.2 V by about 1 order of magnitude, as shown in Figure 4c. In the STM image acquired at 1.4 V (Figure 4d), it becomes difficult to observe a feature similar to that in Figure 4b. At 1.6 V, the feature of the high and the low current states in the  $I-t$  curves becomes unobvious, as shown in Figure 4e. According to the results from the low bias voltages, we attribute this phenomenon to the too fast switching rate at 1.6 V. The bandwidth of the preamplifier of the STM instrument used in this experiment is about 800 Hz, so that the signals with higher frequencies than the bandwidth will be cut off. Hence, the  $I-t$  curve obtained at 1.6 V reflects the average of the high-frequency signals. At 1.6 V, the adsorbed  $O_2$  has a higher dissociation probability, which has been recorded both in the  $I-t$  curves and in the STM images, as shown in Figure 4g,h, respectively. The sudden jump from the high-current state to the low-current state reflects the dissociation of molecular  $O_2$  (Figure 4g). The scratches at opposite  $Ti_{Sc}$  rows are now in the same scanning line, reflecting the excitation of  $O_2$  and dissociation quickly, as shown in parts f (lower right) and h of Figure 4.

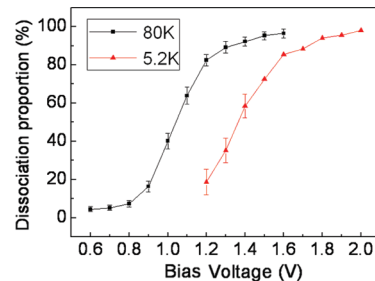


**Figure 5.** Proportion of dissociated  $O_2$  as a function of the applied bias voltages. The error bars give the standard deviation of the data from more than five runs. The data obtained at higher bias voltages at 5.2 K were simply averaged over just two runs, without giving an error bar.

It thus becomes understandable that the nearly symmetric paired protrusions shown in Figure 3c are caused by the fast switching between the flat-lying equilibrium configuration and the inclined configuration, either on the left or on the right side of the tip, as shown in Figure 3g,h, which are symmetric to the equilibrium state. However, the slow scanning process of the STM instrument can only obtain an average signal of the fast switching states in the images. Similar behavior has been observed in our previous study for another molecular system between two switching states excited by the IETE, which is generally through a multiple-electron process.<sup>41</sup> However, due to the low conductivity of  $TiO_2$ , the measurement with a higher tunneling current is difficult. It is currently no possible to decide experimentally whether the IETE-induced dissociation of  $O_2$  is through a multiple-electron process or a single-electron process.

Figure 5 is a plot of the proportion of dissociated  $O_2$  molecules as a function of the applied bias voltage. The proportion of dissociated  $O_2$  is obtained by averaging  $\Delta N/N$  at every bias voltage. In each scanning area of the different experimental runs, we counted the number of dissociated  $O_2$  molecules,  $\Delta N$ . As we have shown above, repeated scanning may induce dissociation of all of the adsorbed molecules even at a not very high bias voltage. To make the data comparable, we counted the number of dissociated  $O_2$  molecules just in the first scanned STM images obtained by using the same scanning speed of 100 nm/s and the same set point current of 10 pA, typically with an area of about  $30 \times 30 \text{ nm}^2$ . The typical  $O_2$  coverage used in such a measurement is about 50% relative to the  $BBO_V$ , where the concentration of  $BBO_V$  is about 8–12%. The total number of adsorbed  $O_2$  molecules also includes the number of dissociative  $O_2$  molecules. It is observed that at 80 K a distinct increase of the proportion appears when the applied bias voltage is higher than 0.8 V, and almost all of the adsorbed  $O_2$  molecules are dissociated even when scanned only once when the voltage is higher than 1.4 V. This may explain the previous STM observations of only dissociative  $O_2$  since in most cases much higher bias voltages were applied.

**4.4. Temperature Dependence of the STM-Tip-Induced  $O_2$  Dissociation.** It has been shown that the  $O_2$  adsorption behavior is temperature dependent.<sup>7,8,27</sup> We have further checked the adsorption behaviors of  $O_2$  at various temperatures. For the  $TiO_2$  surface by dosing  $O_2$  at room temperature, we always observed that  $O_2$  is dissociative.<sup>20</sup> Here, we observed that molecular  $O_2$  can be intrinsically adsorbed at  $BBO_V$  by  $O_2$  dosing at low temperatures, showing coverage dependence. At 80 K, most of the adsorbed molecular  $O_2$  may survive from the tip-induced dissociation at biases lower than 0.8 V. By warming the sample to a

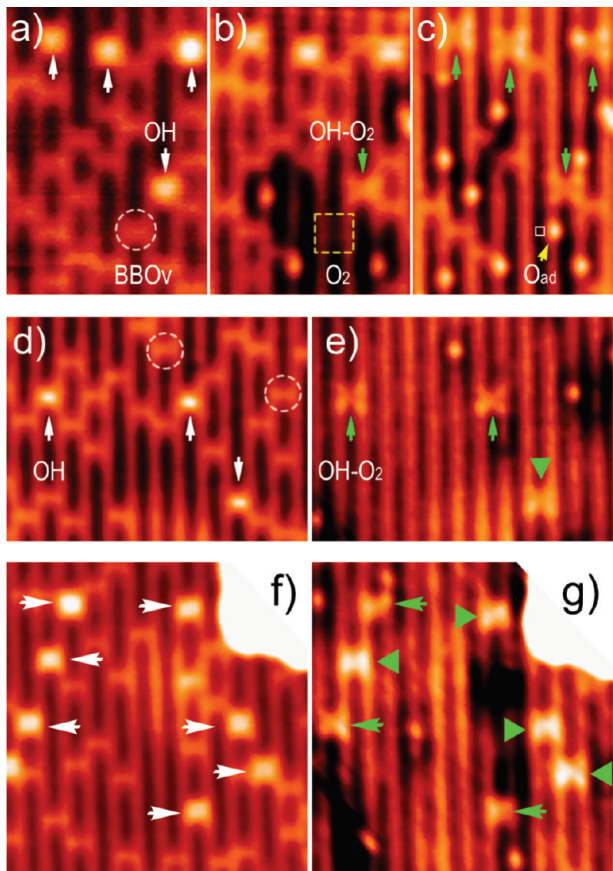


**Figure 6.** (a) Image of the partially hydroxylated  $\text{TiO}_2(110)$ -1×1 surface (size  $4.5 \times 6.5 \text{ nm}^2$ , 1.0 V and 10 pA), (b) image acquired after 0.02 langmuir of  $\text{O}_2$  dosing, and (c) image acquired after an additional 0.05 langmuir of  $\text{O}_2$  dosing. (d, e) Pair of images before and after 0.20 langmuir of  $\text{O}_2$  dosing (size  $8.1 \times 6.0 \text{ nm}^2$ , 1.0 V and 10 pA). (f, g) Pair of images before and after 0.30 langmuir of  $\text{O}_2$  dosing (size  $8.4 \times 8.7 \text{ nm}^2$ , 1.0 V and 10 pA). Key: white arrows, OH; green arrows, OH– $\text{O}_2$  complex; circles, BBO<sub>V</sub>; squares, molecular  $\text{O}_2$  at BBO<sub>V</sub>.

high temperature of 130 K, we still observed the adsorbed molecular  $\text{O}_2$  at BBO<sub>V</sub>, but the proportion of dissociated  $\text{O}_2$  molecules increased to 20% even at a low bias of 0.6 V. Since it took too long to perform the similar measurement at 130 K, instead, we have performed the measurements at a much lower temperature of 5.2 K. At this temperature, we can only image the surface with a bias higher than 1.2 V and a very low set point current of about 10 pA. The data obtained at 5.2 K are also plotted in Figure 5 for comparison with those obtained at 80 K. At 5.2 K, a similar dependence of  $\text{O}_2$  dissociation on the voltage is observed, but for the same value of the proportion, the voltage shifts to a high value by about 0.35 V at 5.2 K. This reflects quite an obvious dissociation dependence on the temperature, in addition to the dependence on the bias voltage.

**4.5. Observation of Molecular  $\text{O}_2$  Adsorbed at Hydroxyl Sites.** The hydroxyl groups have been introduced as another charge donor site to react with  $\text{O}_2$  molecules.<sup>15,42,43</sup> The distribution of the excess electrons of OH has been observed to be similar to that of BBO<sub>V</sub>, which is delocalized to the neighboring  $\text{Ti}_{5c}$  sites.<sup>44</sup> To get insight into the electron scavenging process of molecular  $\text{O}_2$  on the surface, it is also important to understand the interaction between the molecular oxygen and OH. We prepared the clean  $\text{TiO}_2$  sample first and then kept the sample at

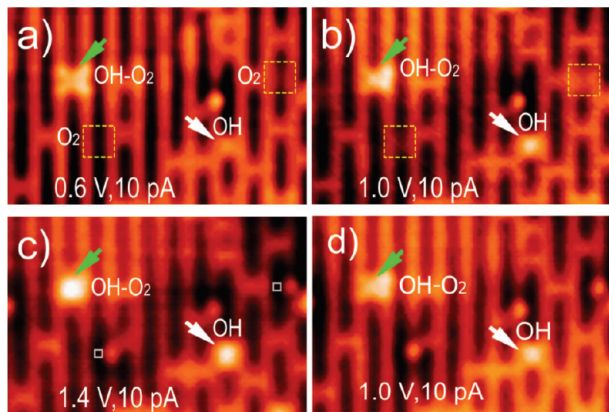


**Figure 7.** Voltage-dependent images of molecular  $\text{O}_2$  adsorbed at OH sites: (a) 0.6 V and 10 pA, (b) 1.0 V and 10 pA, (c) 1.4 V and 10 pA, and (d) 1.0 V and 10 pA after repeated scanning at 1.4 V and 10 pA about 10 times. Size:  $7.5 \times 4.9 \text{ nm}^2$ .

room temperature for about 12 h in a chamber with a base pressure of about  $1 \times 10^{-10}$  mbar before it was transferred to the cryostat of the microscope. In this way, we obtained a partially hydroxylated  $\text{TiO}_2$  surface with a few OH groups in the BBO<sub>V</sub> rows, which were produced from the dissociation of background water in the chamber, as shown in Figure 6a. The surface was then exposed to  $\text{O}_2$  at 80 K. Parts b and c of Figure 6 show the images obtained from the  $\text{O}_2$ -dosed sample in two steps. In the first step, we allowed the surface to be exposed to 0.02 langmuir of  $\text{O}_2$ . Some adsorbed molecular  $\text{O}_2$  and dissociative  $\text{O}_2$  are also observed, similar to our discussion above. Interestingly, it is observed that one of the OH groups changes from a round shape to an X-like shape, as marked by the green arrow in Figure 6b, while the other three OH groups in the upper panel remain unchanged. In the second step, we allowed the surface to be exposed to an additional 0.05 langmuir of  $\text{O}_2$ . The other three remaining OH groups now also change from the round shape to the X-like shape (Figure 6c). The shape change of the OH groups here thus can be directly attributed to the adsorption of, most likely, one  $\text{O}_2$  molecule at each OH, forming a OH– $\text{O}_2$  complex. Generally, such a OH– $\text{O}_2$  complex shows an asymmetric X-like shape at 1.0 V. Similar behaviors have been observed for the 0.2 langmuir of  $\text{O}_2$  dosed sample, as shown in Figure 6d,e. In Figure 6e, all of the BBO<sub>V</sub>s are filled with molecular  $\text{O}_2$ . It is noted that one of the complexes of  $\text{O}_2$  at OH is different from the other two, showing a more protruded and symmetric shape (marked by the triangle). In the sample with a higher exposure of 0.3 langmuir of  $\text{O}_2$ , more complexes with such a shape present, as shown in Figure 6f,g. The complexes with the more protruded and symmetric shape may be due to the OH containing two or more  $\text{O}_2$  molecules. The exact configuration with high coverage of  $\text{O}_2$  adsorbed at OH needs further study.

Here we just discuss OH with only one adsorbed  $\text{O}_2$  molecule. In our previous work, we have shown that OH exhibits a dependence on the bias voltage and the tunneling current in the STM images.<sup>19</sup> A set of STM images acquired at different bias voltages are given in Figure 7. At a low bias voltage of 0.6 V the OH– $\text{O}_2$  complex shows a relatively symmetric X-like shape (Figure 7a). As a comparison, one can see that OH is just slightly more protruded than BBO<sub>V</sub>. At an intermediate bias voltage of 1.0 V the OH– $\text{O}_2$  complex exhibits a asymmetric X-like shape (Figure 7b), and at a high bias voltage of 1.4 V the complex

becomes a very round shape, similar to the protrusion of the OH in the same frame. To confirm that the round-shaped protrusion of the complex is not due to the desorption of O<sub>2</sub> from the complex, we acquired the image back to a low bias voltage of 1.0 V and found that the X-like shape remains, as shown in Figure 7d. At a higher bias voltage of around 2.2 V, we did not observe desorption of O<sub>2</sub> from the complex. The observation here suggests that the adsorbed molecular O<sub>2</sub> at OH is more stable than that at BBO<sub>V</sub> against the IETE. Henderson et al. reported that the O<sub>2</sub> + OH reaction does not occur at low temperatures below 120 K.<sup>45</sup> It is suggested that OH reacts with O<sub>2</sub> at room temperature, yielding an intermediate hydroperoxyl (HO<sub>2</sub>) species at the Ti<sub>Sc</sub> site.<sup>9,24</sup> It is observed that the HO<sub>2</sub> species presents as a protrusion at a Ti<sub>Sc</sub> site. However, in our observation the OH–O<sub>2</sub> complex exhibited at a BBO site shows a dependence quite similar to that of OH on the bias voltage, suggesting that the electronic states of the OH in the complex almost remain as the individual OH. This is consistent with results that O<sub>2</sub> and OH do not react at 80 K. The OH–O<sub>2</sub> complex at 80 K could be a precursor of the HO<sub>2</sub> species.

During the manuscript preparation, we noticed some similar works by other groups.<sup>46,47</sup> Scheiber et al.<sup>46</sup> reported the observation of an elusive adsorbate on the O<sub>2</sub>-dosed TiO<sub>2</sub> surface, which is assigned to the adsorption of molecular O<sub>2</sub>. This is consistent with the misty BBO<sub>V</sub> of singly adsorbed molecular O<sub>2</sub> in our observations (Figures 1 and 2). However, we have an explanation for the O<sub>2</sub> dissociation mechanism quite different from their interpretation. Our results strongly suggest the dissociation of O<sub>2</sub> undergoes an intermediate state, as discussed above, illustrated in Figure 3f–h, and evidenced by the switching behavior as shown in Figure 4. Moreover, our results show that molecular O<sub>2</sub> adsorbed at OH can be very stable and also indicate the existence of stable O<sub>2</sub> adsorbates with the BBO<sub>V</sub> fully filled surface by excess O<sub>2</sub> dosing, different from the dissociative behavior of singly adsorbed O<sub>2</sub> at BBO<sub>V</sub>. A more recent work by Wang et al.<sup>47</sup> reported that molecular O<sub>2</sub> can adsorb both at BBO<sub>V</sub> and at Ti<sub>Sc</sub> sites. They found that molecular O<sub>2</sub> can be observed at Ti<sub>Sc</sub> sites with rather extremely low parameters of the bias voltage and the tunneling current of 0.3 V and 1 pA, respectively, whereas O<sub>2</sub> molecules at Ti<sub>Sc</sub> sites become dissociative at 0.6 V and 1 pA, suggesting a quite easy STM-tip-induced O<sub>2</sub> dissociation process. This may explain our observation of only dissociative O<sub>2</sub> at Ti<sub>Sc</sub> sites since we typically imaged the surface at biases higher than 0.6 V.

## 5. CONCLUSIONS

In conclusion, we have systematically studied the adsorption behaviors of molecular O<sub>2</sub> at BBO<sub>V</sub> on the reduced TiO<sub>2</sub>(110)-1×1 surface using low-temperature STM. We provide direct evidence that molecular O<sub>2</sub> intrinsically adsorbs at the defect sites of BBO<sub>V</sub> and OH of the surface by comparing the performance of the adsorbed O<sub>2</sub>. The adsorbed molecular O<sub>2</sub> at BBO<sub>V</sub> can be dissociated by the IETEs from the STM tip under relatively high bias voltages. The tip-induced dissociation of O<sub>2</sub> undergoes an intermediate state in which the molecular O<sub>2</sub> is excited from its flat-lying equilibrium adsorption site, centered at BBO<sub>V</sub>, to an offset site with an inclined configuration by the IETE. The tip-induced dissociation also shows the dependence on the applied bias voltage and the temperature. Differently, singly adsorbed molecular O<sub>2</sub> at OH can survive from the tip-induced dissociation under relatively high bias voltages, showing

that the adsorbed O<sub>2</sub> at OH is more stable than that at BBO<sub>V</sub>. Our findings here provide useful and important information for the atomic-scale study of O<sub>2</sub>-related chemical processes.

## ■ AUTHOR INFORMATION

### Corresponding Author

bwang@ustc.edu.cn; jghou@ustc.edu.cn

## ■ ACKNOWLEDGMENT

We appreciate the helpful discussion with Prof. Jin Zhao and Prof. Yi Luo. This work was supported by the NBRP (Grant 2011CB921400) and NSFC (Grants 50721091, 90921013, 10825415, 60771006, and 20873129), China.

## ■ REFERENCES

- Dohnálek, Z.; Lyubinetsky, I.; Rousseau, R. *Prog. Surf. Sci.* **2010**, 85, 161.
- Diebold, U. *Surf. Sci. Rep.* **2003**, 48, 53.
- Diebold, U.; Lehman, J.; Mahmoud, T.; Kuhn, M.; Leonardelli, G.; Hebenstreit, W.; Schmid, M.; Varga, P. *Surf. Sci.* **1998**, 411, 137.
- Haruta, M.; Kobayashi, T.; Sano, H.; Yamada, N. *Chem. Lett.* **1987**, 2, 405.
- Thompson, T. L.; Yates, J. T. *Chem. Rev.* **2006**, 106, 4428.
- Lu, G. Q.; Linsebigler, A.; Yates, J. T. *J. Chem. Phys.* **1995**, 102, 4657.
- Wendt, S.; Sprunger, P. T.; Lira, E.; Madsen, G. K. H.; Li, Z. S.; Hansen, J. Ø.; Matthiesen, J.; Blekinge-Rasmussen, A.; Lægsgaard, E.; Hammer, B.; Besenbacher, F. *Science* **2008**, 320, 1755.
- Henderson, M. A.; Epling, W. S.; Perkins, C. L.; Peden, C. H. F.; Diebold, U. *J. Phys. Chem. B* **1999**, 103, 5328.
- Papageorgiou, A. C.; Beglitis, N. S.; Pang, C. L.; Teobaldi, G.; Cabailh, G.; Chen, Q.; Fisher, A. J.; Hofer, W. A.; Thornton, G. *Proc. Natl. Acad. Sci. U.S.A.* **2010**, 107, 2391.
- Tilocca, A.; Selloni, A. *ChemPhysChem* **2005**, 6, 1911.
- Rasmussen, M. D.; Molina, L. M.; Hammer, B. *J. Chem. Phys.* **2004**, 120, 988.
- Lira, E.; Hansen, J. Ø.; Huo, P.; Bechstein, R.; Galliker, P.; Lægsgaard, E.; Hammer, B.; Wendt, S.; Besenbacher, F. *Surf. Sci.* **2010**, 604, 1945.
- Pang, C. L.; Lindsay, R.; Thornton, G. *Chem. Soc. Rev.* **2008**, 37, 2328.
- Cui, X. F.; Wang, B.; Wang, Z.; Huang, T.; Zhao, Y.; Yang, J. L.; Hou, J. G. *J. Chem. Phys.* **2008**, 129, 044703.
- Deskins, N. A.; Rousseau, R.; Dupuis, M. *J. Phys. Chem. C* **2010**, 114, 5891.
- Du, Y. G.; Deskins, N. A.; Zhang, Z. R.; Dohnálek, Z.; Dupuis, M.; Lyubinetsky, I. *Phys. Chem. Chem. Phys.* **2010**, 12, 6337.
- Epling, W. S.; Peden, C. H. F.; Henderson, M. A.; Diebold, U. *Surf. Sci.* **1998**, 412–13, 333.
- Wendt, S.; Schaub, R.; Matthiesen, J.; Vestergaard, E. K.; Wahlström, E.; Rasmussen, M. D.; Thostrup, P.; Molina, L. M.; Lægsgaard, E.; Stensgaard, I.; Hammer, B.; Besenbacher, F. *Surf. Sci.* **2005**, 598, 226.
- Cui, X. F.; Wang, Z.; Tan, S. J.; Wang, B.; Yang, J. L.; Hou, J. G. *J. Phys. Chem. C* **2009**, 113, 13204.
- Wang, Z.; Zhao, Y.; Cui, X.; Tan, S.; Zhao, A.; Wang, B.; Yang, J.; Hou, J. G. *J. Phys. Chem. C* **2010**, 114, 18222.
- Bikondo, O.; Pang, C. L.; Ithnin, R.; Muryn, C. A.; Onishi, H.; Thornton, G. *Nat. Mater.* **2006**, 5, 189.
- Du, Y. G.; Dohnálek, Z.; Lyubinetsky, I. *J. Phys. Chem. C* **2008**, 112, 2649.
- Zhang, Z.; Lee, J.; Yates, J. T.; Bechstein, R.; Lira, E.; Hansen, J. Ø.; Wendt, S.; Besenbacher, F. *J. Phys. Chem. C* **2010**, 114, 3059.

- (24) Du, Y. G.; Deskins, N. A.; Zhang, Z. R.; Dohnálek, Z.; Dupuis, M.; Lyubinetsky, I. *J. Phys. Chem. C* **2009**, *113*, 666.
- (25) Matthiesen, J.; Wendt, S.; Hansen, J. Ø.; Madsen, G. K. H.; Lira, E.; Galliker, P.; Vestergaard, E. K.; Schaub, R.; Lægsgaard, E.; Hammer, B.; Besenbacher, F. *ACS Nano* **2009**, *3*, 517.
- (26) Zhang, Z.; Du, Y.; Petrik, N. G.; Kimmel, G. A.; Lyubinetsky, I.; Dohnálek, Z. *J. Phys. Chem. C* **2009**, *113*, 1908.
- (27) Kimmel, G. A.; Petrik, N. G. *Phys. Rev. Lett.* **2008**, *100*, 196102.
- (28) Pillay, D.; Wang, Y.; Hwang, G. S. *J. Am. Chem. Soc.* **2006**, *128*, 14000.
- (29) Linsebigler, A. L.; Lu, G. Q.; Yates, J. T. *Chem. Rev.* **1995**, *95*, 735.
- (30) Fujishima, A.; Zhang, X. T.; Tryk, D. A. *Surf. Sci. Rep.* **2008**, *63*, 515.
- (31) Petrik, N. G.; Kimmel, G. A. *J. Phys. Chem. Lett.* **2010**, *1*, 1758.
- (32) Kresse, G.; Hafner, J. *Phys. Rev. B* **1993**, *48*, 13115.
- (33) Kresse, G.; Hafner, J. *Phys. Rev. B* **1993**, *47*, 558.
- (34) Kresse, G.; Hafner, J. *Phys. Rev. B* **1994**, *49*, 14251.
- (35) Kresse, G.; Joubert, D. *Phys. Rev. B* **1999**, *59*, 1758.
- (36) Lindan, P. J. D.; Harrison, N. M.; Gillan, M. J.; White, J. A. *Phys. Rev. B* **1997**, *55*, 15919.
- (37) Tersoff, J.; Hamann, D. R. *Phys. Rev. Lett.* **1983**, *50*, 1998.
- (38) Tersoff, J.; Hamann, D. R. *Phys. Rev. B* **1985**, *31*, 805.
- (39) Wang, Y.; Pillay, D.; Hwang, G. S. *Phys. Rev. B* **2004**, *70*, 193410.
- (40) Chrétien, S.; Metiu, H. *J. Chem. Phys.* **2008**, *129*, 074705.
- (41) Pan, S. A.; Fu, Q.; Huang, T.; Zhao, A. D.; Wang, B.; Luo, Y.; Yang, J. L.; Hou, J. G. *Proc. Natl. Acad. Sci. U.S.A.* **2009**, *106*, 15259.
- (42) Liu, L. M.; Crawford, P.; Hu, P. *Prog. Surf. Sci.* **2009**, *84*, 155.
- (43) Petrik, N. G.; Zhang, Z. R.; Du, Y. G.; Dohnálek, Z.; Lyubinetsky, I.; Kimmel, G. A. *J. Phys. Chem. C* **2009**, *113*, 12407.
- (44) Minato, T.; Sainoo, Y.; Kim, Y.; Kato, H. S.; Aika, K.; Kawai, M.; Zhao, J.; Petek, H.; Huang, T.; He, W.; Wang, B.; Wang, Z.; Zhao, Y.; Yang, J. L.; Hou, J. G. *J. Chem. Phys.* **2009**, *130*, 124502.
- (45) Henderson, M. A.; Epling, W. S.; Peden, C. H. F.; Perkins, C. L. *J. Phys. Chem. B* **2003**, *107*, 534.
- (46) Scheiber, P.; Riss, A.; Schmid, M.; Varga, P.; Diebold, U. *Phys. Rev. Lett.* **2010**, *105*, 216101.
- (47) Wang, Z.-T.; Du, Y.; Dohnálek, Z.; Lyubinetsky, I. *J. Phys. Chem. Lett.* **2010**, *1*, 3524.